Research article

Qixin Shen, Amirhassan Shams-Ansari, Andrew M. Boyce, Nathaniel C. Wilson, Tao Cai, Marko Loncar and Maiken H. Mikkelsen*

A metasurface-based diamond frequency converter using plasmonic nanogap resonators

https://doi.org/10.1515/nanoph-2020-0392
Received July 12, 2020; accepted August 30, 2020; published online September 28, 2020

Abstract: Diamond has attracted great interest as an appealing material for various applications ranging from classical to quantum optics. To date, Raman lasers, single photon sources, quantum sensing and quantum communication have been demonstrated with integrated diamond devices. However, studies of the nonlinear optical properties of diamond have been limited, especially at the nanoscale. Here, a metasurface consisting of plasmonic nanogap cavities is used to enhance both $\chi^{(2)}$ and $\chi^{(3)}$ nonlinear optical processes in a wedge-shaped diamond slab with a thickness down to 12 nm. Multiple nonlinear processes were enhanced simultaneously due to the relaxation of phase-matching conditions in subwavelength plasmonic structures by matching two excitation wavelengths with the fundamental and second-order modes of the nanogap cavities. Specifically, third-harmonic generation (THG) and second-harmonic generation (SHG) are both enhanced 1.6×10^7-fold, while four-wave mixing is enhanced 3.0×10^5-fold compared to diamond without the metasurface. Even though diamond lacks a bulk $\chi^{(2)}$ due to centrosymmetry, the observed SHG arises from the surface $\chi^{(2)}$ of the diamond slab and is enhanced by the metasurface elements. The efficient, deeply subwavelength diamond frequency converter demonstrated in this work suggests an approach for conversion of color center emission to telecom wavelengths directly in diamond.

***Corresponding author: Maiken H. Mikkelsen**, Department of Electrical and Computer Engineering, Duke University, Durham, NC, 27708, USA, E-mail: m.mikkelsen@duke.edu. https://orcid.org/0000-0002-0487-7585
Qixin Shen and Nathaniel C. Wilson, Department of Physics, Duke University, Durham, NC, 27708, USA
Amirhassan Shams-Ansari and Marko Loncar, John A. Paulson School of Engineering and Applied Sciences, Harvard University, Cambridge, MA, 02138, USA
Andrew M. Boyce and Tao Cai, Department of Electrical and Computer Engineering, Duke University, Durham, NC, 27708, USA

Keywords: diamond; frequency conversion; nanogap cavity; nonlinear generation; plasmonics.

The unique properties of diamond such as a superior thermal conductivity, a high index of refraction, an ultrawide transparency window and negligible birefringence [1–3] have made this material a promising platform for nanophotonics both in the classical [4–7] and quantum regimes [8–14]. Additionally, with its relatively high third-order nonlinear susceptibility ($\chi^{(3)}$), diamond is an appealing candidate for integrated nonlinear devices. To date, Raman lasing [15, 16], supercontinuum generation [17] and frequency combs [18] have been demonstrated in an integrated, single-crystal diamond platform. One of the distinctive features of diamond is its ability to host defects in its crystal lattice known as color centers, which are key components for quantum communication. These optically addressable spin qubits are unexplored in terms of their interactions with nonlinear processes such as frequency conversion to shift their emission wavelength [19]. However, this task has remained an outstanding challenge due to the weak intrinsic response of nonlinear processes and the phase-matching requirements. Plasmonic structures have proven to be a well-suited platform to investigate and enhance nonlinear optical processes [20–24]. The deeply subwavelength scale of these devices simultaneously allows for large confinement and enhancement of electric fields [25–29], as well as a relaxation of phase-matching conditions [30–32].

Here, film-coupled, plasmonic nanogap cavities created by a nondisruptive transfer method are utilized to enhance the nonlinear response in nanoscale diamond films without patterning the diamond itself. When the excitation wavelength overlaps with the cavity resonance, both third-harmonic generation (THG) and second-harmonic generation (SHG) are dramatically enhanced compared to a thin diamond slab reference. Furthermore, THG, sum frequency generation (SFG) and four-wave mixing (FWM) were enhanced simultaneously by leveraging two different cavity modes, further highlighting the versatility of this platform as a frequency converter.

The diamond slab is sandwiched in between a 75 nm gold film and gold nanoparticles, forming plasmonic nanogap cavities. Arrays of nanoparticles were fabricated on a silicon substrate by electron beam lithography (EBL) and then transferred onto the diamond slab using a polydimethylsiloxane (PDMS) stamp (see Supplementary material for fabrication details). As shown in Figure 1a, there are three key areas on the sample: (A) transferred nanoparticles on a 12-nm-thick diamond film, forming nanogap cavities; (B) transferred nanoparticles on a ~200 nm diamond film, which behave as decoupled nanoparticles due to the increased diamond thickness and (C) diamond (12 nm thick) on a gold substrate, serving as a reference. An additional reference consists of a bare diamond slab on PDMS with a similar thickness and gradient as the diamond slab on gold. The thicknesses of the different areas of the diamond slab are confirmed by atomic force microscopy as shown in Figure 1b. The height profile in Figure 1c demonstrates that the thinnest section of the diamond is 12 nm thick. A schematic of the sample is shown in Figure 1d and consists of arrays of nanoparticles (220 nm particle side length) with a pitch of 440 nm on a wedge-shaped diamond thin film (gradient of ~2.6 nm/μm).

The simulated field distribution for a nanocavity with a 12 nm diamond gap illustrates that the highly confined electric fields in the cavity are enhanced up to 40-fold in comparison with the original incident field, facilitating enhanced nonlinear generation (Figure 1e). A reflection spectrum is measured from 700 to 1600 nm to determine the cavities' resonance wavelengths. For the nanogap cavities, the fundamental resonance mode is at 1455 nm and the second-order mode is at 840 nm (Figure 1f). The fundamental mode is blue shifted to 1130 nm for the decoupled nanoparticles, and no obvious second-order mode is observed. We attribute the fundamental mode from the decoupled nanoparticles to a localized surface plasmon resonance (LSPR) mode from the nanoparticle itself. This mode is distinct from the gap mode in nanogap cavities because the ~200 nm separation between the gold nanoparticles and substrate is too thick to support gap plasmons.

To leverage the field enhancement in the nanogap cavities for nonlinear generation, a pump wavelength of 1455 nm, matching the fundamental cavity resonance, is used to excite THG. The presence of THG is confirmed via observation of a third-order power law during power dependence measurements on all three regions of the sample and on the control as shown in Figure 2a. The THG response from the nanogap cavities is enhanced 1.6×10^7-fold compared to bare diamond on PDMS (details on calculation of enhancement factor in Supplementary material). Next, to investigate if the large enhancement is arising from the nanogap mode or simply the presence of the gold nanoparticles, THG is also measured from the decoupled nanoparticles. Measurements are performed using both 1455 nm excitation, which overlaps with the fundamental resonance of the nanogap mode (Figure 2a), and 1130 nm excitation, which overlaps with the LSPR mode of the decoupled nanoparticles (Figure 2b). For the decoupled nanoparticles, nearly three orders of magnitude less enhancement is observed for both excitation wavelengths, even though a larger amount of nonlinear medium (i.e. a thicker diamond layer) contributes to the THG response. The electric field intensity is much less in the diamond for the decoupled nanoparticles, resulting in less THG enhancement.

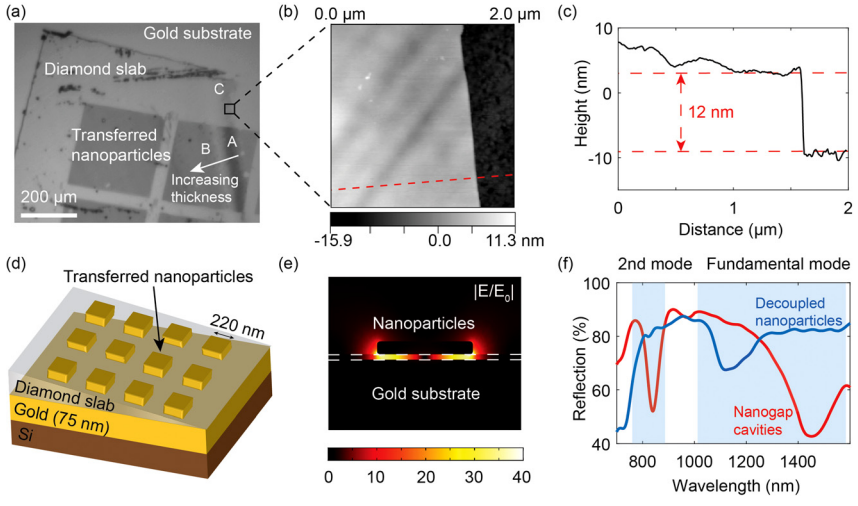

Figure 1: (a) Optical image of the sample. Area A: transferred nanoparticles on ~12 nm diamond, forming nanogap cavities; area B: transferred nanoparticles on ~200 nm diamond, forming decoupled nanoparticles; area C: diamond on gold. (b) Atomic force microscopy (AFM) image of the area in (a) delineated by the square. (c) Height profile along the red, dashed line in (b). (d) Schematic of the sample structure: a thin diamond wedge is sandwiched in between a 75 nm evaporated gold film and electron beam lithography (EBL)–fabricated gold nanoparticles with a height of 30 nm. (e) Simulated electric field enhancement distribution of nanogap cavities at 1455 nm. (f) Measured reflection spectra from nanogap cavities (red) and decoupled nanoparticles (blue).

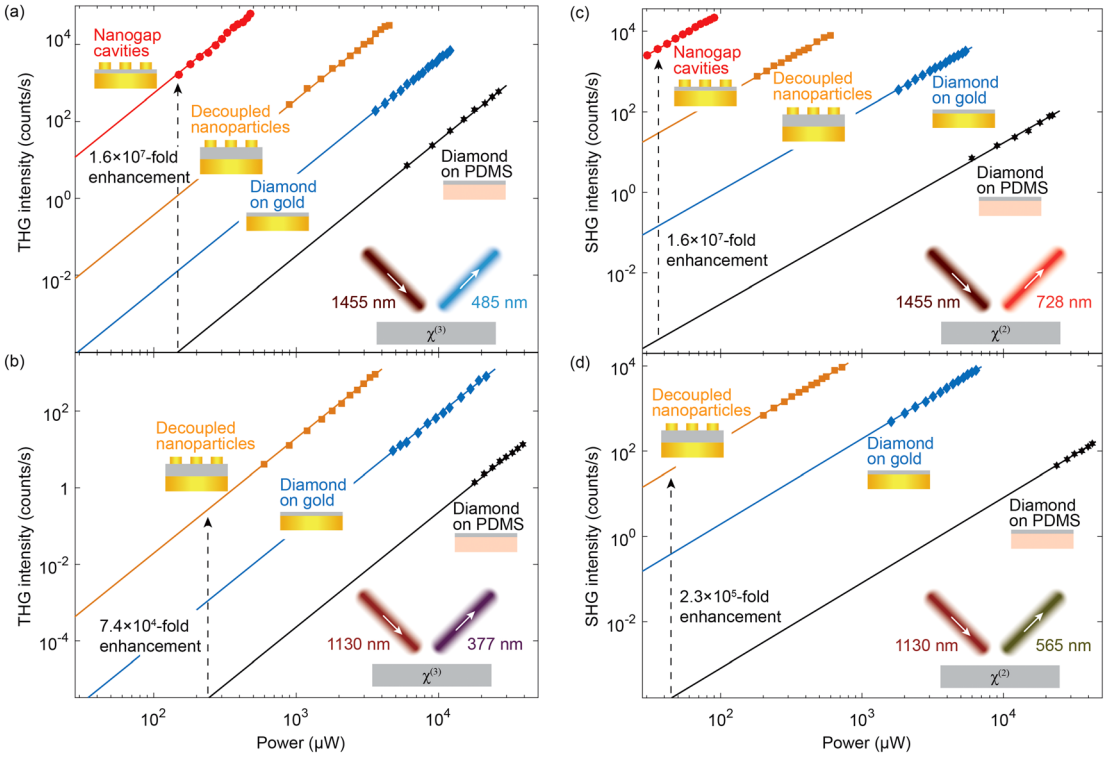

Figure 2: (a and b) Third-harmonic generation (THG) intensity as a function of excitation power shown on a log scale. Data points are experimental results, and lines are cubic polynomial fits. (a) 1455 nm excitation. (b) 1130 nm excitation. (c and d) Second-harmonic generation (SHG) intensity as a function of excitation power shown on a log scale. Data points are experimental results, and lines are quadratic polynomial fits. (c) 1455 nm excitation. (d) 1130 nm excitation. Nanogap cavities: transferred nanoparticles on ~12 nm diamond with an underlying gold film; decoupled nanoparticles: transferred nanoparticles on ~200 nm diamond with an underlying gold film.

As seen in Figure 2a and b, the nonlinear response from the diamond on gold is also enhanced compared with the diamond on PDMS. This may be explained by a contribution from the nonlinearity of gold or surface effects, as the nonlinear response from PDMS itself is negligible. In addition to the large enhancement, the nanogap cavities have relatively high nonlinear conversion efficiencies considering their nanoscale dimensions. The efficiency is defined as the power of the generated nonlinear intensity from embedded diamond nanocavities divided by the power of the incident excitation. The power of the nonlinear signal is derived from the photon counts and a calibrated light source (Labsphere) positioned at the focal plane of the objective lens (details on determining the efficiency in Supplementary material). With an observed damage threshold of 5 mW of excitation power, the maximum THG conversion efficiency is estimated to be 2.33×10^{-5}%.

Similarly, power dependence measurements are performed for SHG, and a quadratic power dependence is observed for both 1455 nm excitation and 1130 nm excitation (Figure 2c and d). SHG is enhanced 1.6×10^7-fold for diamond in the nanogap cavities compared with bare diamond on PDMS for 1455 nm excitation. This enhancement is comparable to the observed THG enhancement even though it is from a lower order nonlinear process. This can be explained by the modified $\chi^{(2)}$ profile within diamond due to the presence of plasmonic structures, giving rise to a higher SHG intensity than simply the enhancement resulting from the electric field confinement in the cavity. The maximum SHG conversion efficiency from the nanogap cavities for a 5 mW excitation power is estimated to be 7.59×10^{-6}%.

Next, the excitation wavelength was varied to further investigate the importance of the plasmonic nanogap mode for enhanced nonlinear responses. Specifically, laser excitation at wavelengths ranging from 1430 to 1480 nm with constant power is utilized for nanogap cavities, and the resulting spectra are shown in Figure 3a for THG and Figure 3b for SHG (additional data in Supplementary material). As expected, the maximum nonlinear intensity occurs at the cavity resonance wavelength (1455 nm) for both the THG and SHG signals. The nonlinear intensity decreases dramatically when the excitation is detuned from 1455 nm due to the reduced electric field intensity

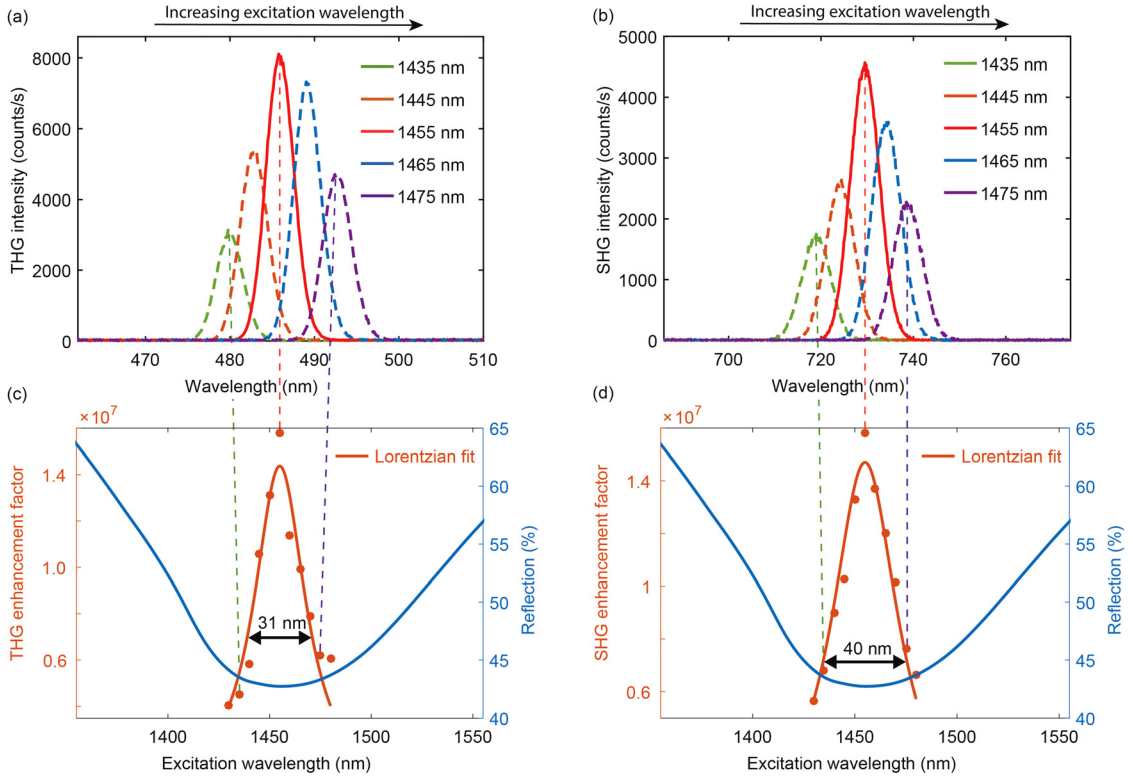

Figure 3: (a) THG response spectra as a function of excitation wavelength. (b) SHG response spectra as a function of excitation wavelength. (c) THG enhancement factor as a function of excitation wavelength (red) compared to the reflection spectrum (blue) which shows the plasmon resonance. The full widths at half maximum (FWHM) of the THG enhancement is 31 nm. (d) SHG enhancement factor as a function of excitation wavelength (red) compared to the reflection spectrum (blue) which shows the plasmon resonance. The FWHM of the SHG enhancement is 40 nm, while the FWHM of the reflection spectrum is 204 nm in both (c) and (d). THG, third-harmonic generation; SHG, second-harmonic generation.

within the diamond layer. Thus, the nonlinear intensity is strongly related to the enhanced electric field intensity confined within the diamond, illustrating that the observed nonlinear response mainly originates from the diamond. The full widths at half maximum (FWHM) of the THG and SHG enhancement as a function of excitation wavelength are noted to be much narrower than the cavity reflection spectrum as shown in Figure 3c and 3d, which is a consequence of the nonlinear dependence of THG and SHG intensity on the electric field intensity. It is observed that THG decreases more rapidly than SHG when the excitation wavelength is detuned from the cavity resonance as the THG depends on the third power of the electric field in the cavity, whereas SHG has a second-order power dependence. THG is expected to have a third-order Lorentzian lineshape and SHG a second-order Lorentzian lineshape. A coupled mode theory analysis gives a ratio between the FWHM of the THG and SHG enhancement of $\frac{\sqrt{\sqrt[3]{2}-1}}{\sqrt{\sqrt{2}-1}} = 0.79$ which agrees very well with the experimentally observed ratio of $\frac{31}{40} = 0.78$ (further details in Supplementary material).

Next, we investigate nonlinear light generation arising from multiple nonlinear optical processes occurring simultaneously within a single nanocavity. Here, SFG and FWM are selected to demonstrate this capability along with the previously characterized THG process. Excitation wavelengths of 840 nm (ω_1) and 1455 nm (ω_2), matching the cavities' fundamental and second-order modes, were selected. The output SFG frequency equals $\omega_{SFG} = \omega_1 + \omega_2$ while the degenerate FWM frequency equals $\omega_{FWM} = 2\omega_1 - \omega_2$ (indicated in the inset schematic in Figure 4c–f).

A variable delay stage is employed to control the relative time delay between the two excitation pulses. The SFG (532 nm) and FWM (590 nm) responses start to appear when the time delay between the two excitation pulses is below approximately 150 fs, which is the pulse duration of the excitation laser. The THG intensity remains constant as it only depends on the 1455 nm excitation (Figure 4a). The largest SFG and FWM intensities are observed at zero time delay when the two excitation pulses are perfectly overlapped (Figure 4b). The emission peak observed at 485 nm is from THG as confirmed above. Similar power dependence measurements are performed to demonstrate that

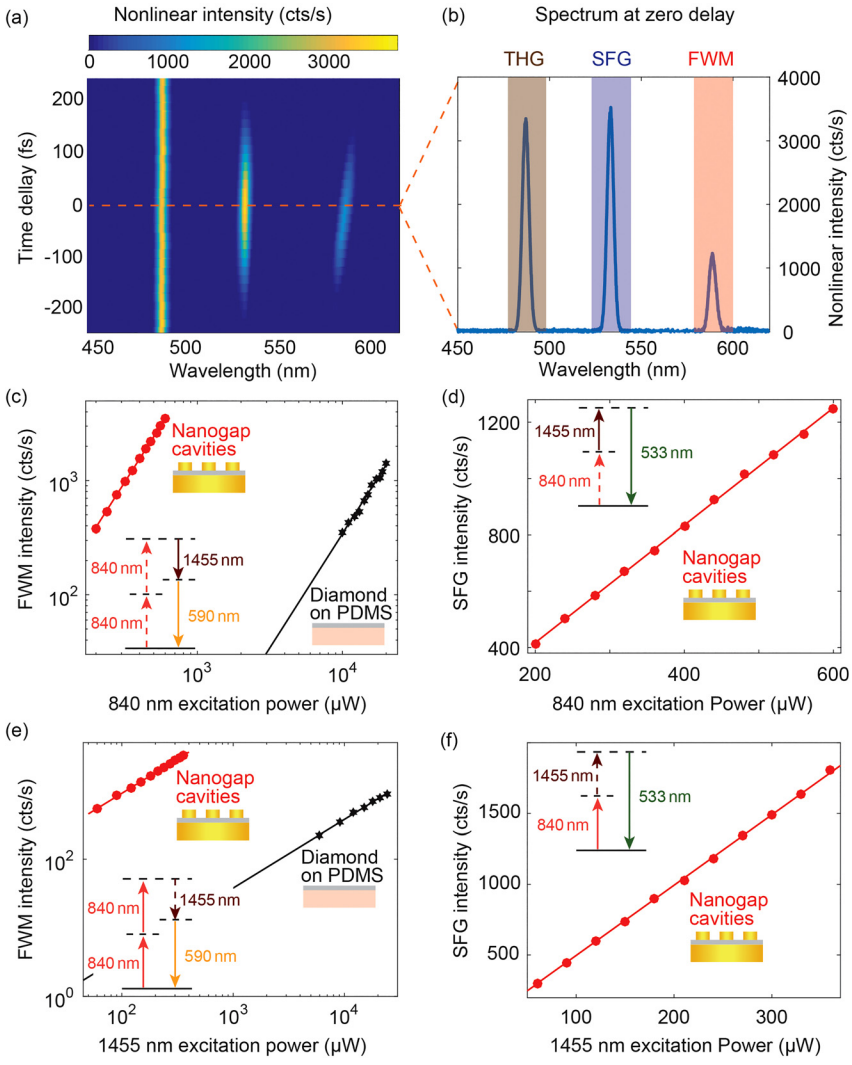

Figure 4: (a) The spectra of nonlinear responses as a function of the time delay between the two excitation pulses at 840 and 1455 nm. (b) Nonlinear response spectra at zero time delay. The three peaks correspond to THG, SFG and FWM as indicated in the figure. (c and d) Power dependence measurements for variable 840 nm excitation power. (c) FWM intensity. The 1455 nm excitation powers for nanogap cavities and the diamond reference are 180 μW and 18 mW, respectively. (d) SFG intensity. The 1455 nm excitation power for nanogap cavities is 180 μW, and SFG intensity from the diamond reference is too small to observe. (e and f) Power dependence measurements for variable 1455 nm excitation power. (e) FWM intensity. The 840 nm excitation powers for nanogap cavities and the diamond reference are 400 μW and 14 mW, respectively. (f) SFG intensity. The 840 nm excitation power for nanogap cavities is 400 μW, and the SFG intensity from the diamond reference is too small to observe. The insets in (c–f) show the energy diagram for the corresponding frequency conversion process. THG, third-harmonic generation; SHG, second-harmonic generation; SFG, sum frequency generation; FWM, four-wave mixing.

the other two peaks are from SFG and FWM processes. Specifically, the signal at the longest wavelength (590 nm) scales quadratically with the 840 nm excitation power and scales linearly with the 1455 nm excitation power. Therefore, it is confirmed that this signal is from FWM as it obeys the expected power law and, furthermore, occurs at the wavelength given by the frequency conversion relation. Similarly, the signal in the middle at 532 nm scales linearly with both the 840 and 1455 nm excitation powers, indicating that it is indeed from SFG.

Large enhancement is expected for SFG and FWM from diamond embedded in the nanogap cavities due to the strong electric field at both excitation wavelengths. Experimentally, we find that FWM is enhanced 3.0×10^5-fold compared to bare diamond on PDMS as extracted from Figures 4c and e. For SFG, the signal from bare diamond is too weak to detect since only the surface of diamond contributes SFG due to the inversion symmetry in its crystal lattice. Thus, we cannot determine an enhancement factor for this process.

In summary, we embed a diamond slab into plasmonic nanogap cavities formed by a gold ground plane and EBL-fabricated nanoparticles transferred using a PDMS stamp. By overlapping the excitation wavelength with the nanocavities' resonance wavelength, 1.6×10^7-fold enhancement is observed for both THG and SHG. This large enhancement is accompanied by relatively high nonlinear conversion efficiencies, approaching 2.33×10^{-5}% and 7.59×10^{-6}% for THG and SHG, respectively. These efficiencies are comparable with other reported results using plasmonic structures [20, 22, 24, 32–34] but achieved with a unique material – diamond – which have not previously been experimentally demonstrated. Furthermore, simultaneous enhancement of multiple nonlinear processes was demonstrated, specifically THG, SFG and FWM, enabled by the relaxed phase-matching

conditions in the deeply subwavelength cavities. To further enhance nonlinear generation, the damage threshold of the structure could be increased by utilizing refractory materials [35–37] such as TiN or gold nanoparticles coated with an ultrathin atomic layer deposition (ALD) layer to prevent deformation [38]. The PDMS transfer process provides a convenient and nondisruptive method to place nanoparticles. This technique, along with the cavity's vertically oriented gap, offers the potential to embed diamond containing color centers. These studies demonstrate a metasurface-based diamond frequency converter that is promising for on-chip nonlinear devices and single-photon frequency conversion of the emission of color centers in diamond from visible to telecommunication wavelengths.

Acknowledgments: M.H.M. acknowledges support from the National Science Foundation (NSF) Grant Numbers EFMA-1640986 and DMR-1454523. M.L. acknowledges support from the Air Force Office of Scientific Research (FA9550-19-1-0376), the Defense Advanced Research Projects Agency (W31P4Q-15-1-0013), and the National Science Foundation (DMR-1231319). Authors acknowledge Pawel Latawiec for developing the diamond thin-film on insulator process.

Author contribution: All the authors have accepted responsibility for the entire content of this submitted manuscript and approved submission.

Research funding: M.H.M. acknowledges support from the National Science Foundation (NSF) Grant Numbers EFMA-1640986 and DMR-1454523. M.L. acknowledges support from the Air Force Office of Scientific Research (FA9550-19-1-0376), the Defense Advanced Research Projects Agency (W31P4Q-15-1-0013), and the National Science Foundation (DMR-1231319).

Conflict of interest statement: The authors declare no conflicts of interest regarding this article.

References

[1] I. Aharonovich, A. D. Greentree, and S. Prawer, "Diamond photonics," *Nat. Photonics*, vol. 5, no. 7, pp. 397–405, 2011.

[2] R. P. Mildren and J. R. Rabeau, *Optical Engineering of Diamond*, John Wiley & Sons, 2013.

[3] A. A. Kaminskii, V. G. Ralchenko, and V. I. Konov, "CVD-diamond – a novel $\chi^{(3)}$-nonlinear active crystalline material for SRS generation in very wide spectral range," *Laser Phys. Lett.*, vol. 3, no. 4, pp. 171–177, 2006.

[4] M. J. Burek, Y. Chu, M. S. Z. Liddy, et al., "High quality-factor optical nanocavities in bulk single-crystal diamond," *Nat. Commun.*, vol. 5, no. 1, pp. 1–7, 2014.

[5] H. A. Atikian, P. Latawiec, M. J. Burek, et al., "Freestanding nanostructures via reactive ion beam angled etching," *APL Photonics*, vol. 2, no. 5, p. 051301, 2017.

[6] F. Gao, J. Van Erps, Z. Huang, H. Thienpont, R. G. Beausoleil, and N. Vermeulen, "Directional coupler based on single-crystal diamond waveguides," *IEEE J. Sel. Top. Quantum Electron.*, vol. 24, no. 6, p. 6100909, 2018.

[7] B. Khanaliloo, M. Mitchell, A. C. Hryciw, and P. E. Barclay, "High-Q/V monolithic diamond microdisks fabricated with quasi-isotropic etching," *Nano Lett.*, vol. 15, no. 8, pp. 5131–5136, 2015.

[8] K. Bray, D. Y. Fedyanin, I. A. Khramtsov, et al., "Electrical excitation and charge-state conversion of silicon vacancy color centers in single-crystal diamond membranes," *Appl. Phys. Lett.*, vol. 116, no. 10, p. 101103, 2020.

[9] S. I. Bogdanov, M. Y. Shalaginov, A. S. Lagutchev, et al., "Ultrabright room-temperature sub-nanosecond emission from single nitrogen-vacancy centers coupled to nanopatch antennas," *Nano Lett.*, vol. 18, no. 8, pp. 4837–4844, 2018.

[10] L. Li, T. Schröder, E. H. Chen, et al., "Coherent spin control of a nanocavity-enhanced qubit in diamond," *Nat. Commun.*, vol. 6, no. 1, pp. 1–7, 2015.

[11] Y. I. Sohn, S. Meesala, B. Pingault, et al., "Controlling the coherence of a diamond spin qubit through its strain environment," *Nat. Commun.*, vol. 9, no. 1, pp. 1–6, 2018.

[12] H. Siampour, O. Wang, V. A. Zenin, et al., "Ultrabright single-photon emission from germanium-vacancy zero-phonon lines: deterministic emitter-waveguide interfacing at plasmonic hot spots," *Nanophotonics*, vol. 9, no. 4, pp. 953–962, 2020.

[13] R. E. Evans, M. K. Bhaskar, D. D. Sukachev, et al., "Photon-mediated interactions between quantum emitters in a diamond nanocavity," *Science (80-)*, vol. 362, no. 6415, pp. 662–665, 2018.

[14] T. Schröder, S. L. Mouradian, J. Zheng, et al., "Quantum nanophotonics in diamond [invited]," *J. Opt. Soc. Am. B*, vol. 33, no. 4, p. B65, 2016.

[15] P. Latawiec, V. Venkataraman, M. J. Burek, B. J. M. Hausmann, I. Bulu, and M. Lončar, "On-chip diamond Raman laser," *Optica*, vol. 2, no. 11, p. 924, 2015.

[16] P. Latawiec, V. Venkataraman, A. Shams-Ansari, M. Markham, and M. Loncar, "An integrated diamond Raman laser pumped in the near-visible," *Opt. Lett.*, vol. 43, no. 2, pp. 318–321, 2017.

[17] A. Shams-Ansari, P. Latawiec, Y. Okawachi, et al., "Supercontinuum generation in angle-etched diamond waveguides," *Opt. Lett.*, vol. 44, no. 16, pp. 4056–4059, 2019.

[18] B. J. M. Hausmann, I. Bulu, V. Venkataraman, P. Deotare, and M. Loncar, "Diamond nonlinear photonics," *Nat. Photonics*, vol. 8, no. 5, pp. 369–374, 2014.

[19] Z. Lin, S. G. Johnson, A. W. Rodriguez, and M. Loncar, "Design of diamond microcavities for single photon frequency down-conversion," *Opt. Express*, vol. 23, no. 19, p. 25279, 2015.

[20] H. Aouani, M. Rahmani, M. Navarro-Cía, and S. A. Maier, "Third-harmonic-upconversion enhancement from a single semiconductor nanoparticle coupled to a plasmonic antenna," *Nat. Nanotechnol.*, vol. 9, no. 4, pp. 290–294, 2014.

[21] P. Genevet, J. P. Tetienne, E. Gatzogiannis, et al., "Large enhancement of nonlinear optical phenomena by plasmonic nanocavity gratings," *Nano Lett.*, vol. 10, no. 12, pp. 4880–4883, 2010.

[22] Q. Shen, T. B. Hoang, G. Yang, V. D. Wheeler, and M. H. Mikkelsen, "Probing the origin of highly-efficient third-

harmonic generation in plasmonic nanogaps," *Opt. Express*, vol. 26, no. 16, pp. 20718–20725, 2018.
[23] Y. Zhang, F. Wen, Y.-R. Zhen, P. Nordlander, and N. J. Halas, "Coherent fano resonances in a plasmonic nanocluster enhance optical four-wave mixing," *Proc. Natl. Acad. Sci.*, vol. 110, no. 23, pp. 9215–9219, 2013.
[24] M. Celebrano, X. Wu, M. Baselli, et al., "Mode matching in multiresonant plasmonic nanoantennas for enhanced second harmonic generation," *Nat. Nanotechnol.*, vol. 10, no. 5, pp. 412–417, 2015.
[25] J. B. Lassiter, F. McGuire, J. J. Mock, et al., "Plasmonic waveguide modes of film-coupled metallic nanocubes," *Nano Lett.*, vol. 13, no. 12, pp. 5866–5872, 2013.
[26] G. M. Akselrod, C. Argyropoulos, T. B. Hoang, et al., "Probing the mechanisms of large purcell enhancement in plasmonic nanoantennas," *Nat. Photonics*, vol. 8, no. 11, pp. 835–840, 2014.
[27] Q. Shen, A. M. Boyce, G. Yang, and M. H. Mikkelsen, "Polarization-controlled nanogap cavity with dual-band and spatially overlapped resonances," *ACS Photonics*, vol. 6, no. 8, pp. 1916–1921, 2019.
[28] J. J. Baumberg, J. Aizpurua, M. H. Mikkelsen, and D. R. Smith, "Extreme nanophotonics from ultrathin metallic gaps," *Nat. Mater.*, vol. 18, no. 7, pp. 668–678, 2019.
[29] A. Rose, T. B. Hoang, F. McGuire, et al., "Control of radiative processes using tunable plasmonic nanopatch antennas," *Nano Lett.*, vol. 14, no. 8, pp. 4797–4802, 2014.
[30] G. Sartorello, N. Olivier, J. Zhang, et al., "Ultrafast optical modulation of second- and third-harmonic generation from cut-disk-based metasurfaces," *ACS Photonics*, vol. 3, no. 8, pp. 1517–1522, 2016.
[31] S. Liu, P. P. Vabishchevich, A. Vaskin, et al., "An all-dielectric metasurface as a broadband optical frequency mixer," *Nat. Commun.*, vol. 9, no. 1, pp. 1–6, 2018.
[32] Q. Shen, W. Jin, G. Yang, A. W. Rodriguez, and M. H. Mikkelsen, "Active control of multiple, simultaneous nonlinear optical processes in plasmonic nanogap cavities," *ACS Photonics*, vol. 7, no. 4, pp. 901–907, 2020.
[33] S. Park, J. W. Hahn, and J. Y. Lee, "Doubly resonant metallic nanostructure for high conversion efficiency of second harmonic generation," *Opt. Express*, vol. 20, no. 5, p. 4856, 2012.
[34] Y. Zhang, N. K. Grady, C. Ayala-Orozco, and N. J. Halas, "Three-dimensional nanostructures as highly efficient generators of second harmonic light," *Nano Lett.*, vol. 11, no. 12, pp. 5519–5523, 2011.
[35] G. Albrecht, M. Ubl, S. Kaiser, H. Giessen, and M. Hentschel, "Comprehensive study of plasmonic materials in the visible and near-infrared: linear, refractory, and nonlinear optical properties," *APL Photonics*, vol. 5, no. 3, pp. 1058–1067, 2018.
[36] U. Guler, A. Boltasseva, and V. M. Shalaev, "Refractory plasmonics," *Science (80-.)*, vol. 344, no. 6181, pp. 263–264, 2014.
[37] M. P. Wells, R. Bower, R. Kilmurray, et al., "Temperature stability of thin film refractory plasmonic materials," *Opt. Express*, vol. 26, no. 12, p. 15726, 2018.
[38] G. Albrecht, S. Kaiser, H. Giessen, and M. Hentschel, "Refractory plasmonics without refractory materials," *Nano Lett.*, vol. 17, no. 10, pp. 6402–6408, 2017.

Supplementary Material: The online version of this article offers supplementary material (https://doi.org/10.1515/nanoph-2020-0392).